frontiers | Frontiers in Marine Science

TYPE Original Research
PUBLISHED 05 July 2023
DOI 10.3389/fmars.2023.1181351

OPEN ACCESS

EDITED BY
Rob Middag,
Royal Netherlands Institute for Sea Research (NIOZ), Netherlands

REVIEWED BY
Yang Xiang,
University of Washington, United States
Daniel Ohnemus,
University of Georgia, United States

*CORRESPONDENCE
Moritz Baumann
mbaumann@geomar.de

RECEIVED 07 March 2023
ACCEPTED 31 May 2023
PUBLISHED 05 July 2023

CITATION
Baumann M, Goldenberg SU, Taucher J, Fernández-Méndez M, Ortiz J, Haussmann J and Riebesell U (2023) Counteracting effects of nutrient composition (Si:N) on export flux under artificial upwelling.
Front. Mar. Sci. 10:1181351.
doi: 10.3389/fmars.2023.1181351

Counteracting effects of nutrient composition (Si:N) on export flux under artificial upwelling

Moritz Baumann[1]*, Silvan Urs Goldenberg[1], Jan Taucher[1], Mar Fernández-Méndez[2], Joaquin Ortiz[1], Jacqueline Haussmann[1] and Ulf Riebesell[1]

[1]Biological Oceanography, GEOMAR Helmholtz Centre for Ocean Research, Kiel, Germany, [2]Biosciences, Polar Biological Oceanography, Alfred-Wegener-Institut Helmholtz-Zentrum für Polar- und Meeresforschung, Bremerhaven, Germany

To keep global warming below 1.5°C, technologies that remove carbon from the atmosphere will be needed. Ocean artificial upwelling of nutrient-rich water stimulates primary productivity and could enhance the biological carbon pump for natural CO_2 removal. Its potential may depend on the Si availability in the upwelled water, which regulates the abundance of diatoms that are key carbon exporters. In a mesocosm experiment, we tested the effect of nutrient composition (Si relative to N) in artificially upwelled waters on export quantity and quality in a subtropical oligotrophic environment. Upwelling led to a doubling of exported particulate matter and increased C:N ratios to well beyond Redfield (9.5 to 11.1). High Si availability stimulated this carbon over-consumption further, resulting in a temporary ~5-fold increase in POC export and ~30% increase in C:N ratios compared to Si-scarce upwelling. Whilst the biogenic Si ballast of the export flux increased more than 3.5-fold over the Si:N gradient, these heavier particles did not sink faster. On the contrary, sinking velocity decreased considerably under high Si:N, most likely due to reduced particle size. Respiration rates remained similar across all treatments indicating that biogenic Si did not protect particles against microbial degradation. Si availability thus influenced key processes of the biological carbon pump in counteracting ways by increasing the export magnitude and associated C:N ratios but decreasing the efficiency of carbon transfer to depth. These opposing effects need to be considered when evaluating the potential of artificial upwelling as negative emission technology.

KEYWORDS

artificial upwelling, biological carbon pump, particulate matter export, sinking velocity, remineralization rate, carbon sequestration, diatoms, mesocosms

1 Introduction

Carbon dioxide removal (CDR) on a grand scale is likely to be a critical component of any feasible plan to keep global warming below 1.5°C (IPCC, 2018). The oceanic realm constitutes the biggest non-geological carbon reservoir of our planet, and it offers vast space for carbon dioxide removal techniques to be deployed. Artificial upwelling is one such technology, which aims to enhance biological productivity in the surface ocean by transporting nutrient-rich water from deeper layers to the oligotrophic surface (Pan et al., 2016). Much like in natural upwelling systems, the increase in primary productivity should theoretically cause an enhanced vertical export flux of sinking particulate organic matter, which transports organically bound carbon to depth. Once the carbon reaches the deep ocean (generally below 1,000 m), it is regarded as sequestered on the time scale of up to centuries (Siegel et al., 2021). This natural process is called the "biological carbon pump" (e.g. Volk and Hoffert, 1985), whose strength might be enhanced using artificial upwelling.

The carbon sequestration potential of artificial upwelling via the biological carbon pump is mainly determined by (a) how much material sinks out of the surface ocean, (b) the efficiency with which it is transferred to depth, i.e. the vertical carbon flux attenuation (Henson et al., 2012a), and (c) the carbon to nutrient ratio of sequestered particulate matter. The first is affected by the pelagic community composition and productivity. The export efficiency is controlled by the velocity with which exported material sinks and the rate at which it is remineralized back to the dissolved inorganic carbon (DIC) pool (McDonnell et al., 2015). The exported matter carbon to nutrient ratio is affected by the community composition in the surface (Coale et al., 2004) and remineralization processes in the sub-surface (Boyd and Trull, 2007). It is critical because the upwelled water contains not only excess nutrients but also excess DIC, which needs to be compensated for (e.g. Oschlies et al., 2010). When all upwelled nutrients are eventually exported, the carbon to nutrient ratio of sequestered matter needs to be higher than that of the upwelled nutrients (e.g. excess DIC : NO_3^-) to achieve net carbon sequestration (Baumann et al., 2021).

Nutrient composition shapes phytoplankton community structure, with implications for food webs and ultimately ecosystem services, such as carbon export. The relative availability of dissolved silicate (orthosilicic acid, $Si(OH)_4$) is perhaps the most important characteristic when it comes to defining the phytoplankton community structure under meso- or eutrophic conditions. Under abundant silicate, diatoms (*Bacillariophyceae*) thrive, whereas under Si scarcity usually phyto-flagellates dominate (Sommer, 1994).

Diatoms are important players in the ocean carbon cycle (Field et al., 1998), contributing 40% to the global particulate organic carbon (POC) export (Jin et al., 2006). Many species are chain-forming, especially those constituting the yearly spring blooms at high latitudes and seasonal blooms in coastal upwelling regions (Smetacek, 1985; Smetacek, 1999). When the limiting nutrient is exhausted (usually nitrate or silicic acid), they form aggregates and export large amounts of biogenic carbon from the euphotic zone to the deep sea (Honjo and Manganini, 1993). Diatom blooms are short-lived, but can be sustained by recurring silicic acid fertilization and the associated carbon sequestration upheld on time scales of weeks to months (Dugdale and Wilkerson, 1998; Allen et al., 2005). Diatoms incorporate the silicic acid into their cell walls as biogenic silica (BSi, opal), a biomineral twice as heavy as particulate organic carbon (Klaas and Archer, 2002). As biogenic ballast material, it is considered to increase particle sinking velocities (Armstrong et al., 2009) and it might as well act as a protective barrier against microbial remineralization (Armstrong et al., 2002; Klaas and Archer, 2002). Furthermore, aggregation processes can be facilitated by the exudation of transparent exopolymer particles (TEP), which are often exuded at the termination of a bloom (Obernosterer and Herndl, 1995) and promote the formation of larger marine snow particles. This suggests that increased Si availability and consequently higher diatom abundances would increase the transfer efficiency of biogenic matter to depth.

However, diatoms do not necessarily promote efficient carbon export. In fact, their blooms can result in relatively inefficient transfer of particulate organic matter from the surface ocean to depth (Guidi et al., 2009; Henson et al., 2012b; Maiti et al., 2013). Exuded TEP itself is positively buoyant and can thus decrease the density of particulate matter in aggregates, thereby leading to its retention in the surface (Mari et al., 2017). Furthermore, diatom-originated aggregates are usually relatively porous, which can reduce sinking velocities and facilitate bacterial remineralization rates (Lam et al., 2011; Puigcorbé et al., 2015; Bach et al., 2019). How these positive and negative effects on carbon export will balance out during artificial upwelling is uncertain.

We here investigate the carbon sequestration potential of artificial upwelling under varying levels of Si availability and diatom dominance. In a mesocosm experiment in the subtropical North Atlantic, we fertilized a natural oligotrophic plankton community with nutrient-rich deep water composed of different Si:N ratios (gradient from 0.07–1.33 mol:mol). During the month-long experiment, Si availability altered plankton community properties in potentially beneficial ways regarding carbon sequestration (Goldenberg et al., 2022). Our study tests how these changes in the surface water were carried over to key export properties including the flux, composition, velocity and remineralization of sinking biogenic matter. By linking plankton communities to the functioning of the biological carbon pump, we characterize the role of diatoms during carbon export and evaluate artificial upwelling as a negative emission technology.

2 Materials and methods

2.1 Experimental setup

The 35 day-long mesocosm experiment was carried out in autumn 2019 in the subtropical North Atlantic. Inside the harbor of Taliarte, Spain (27°59'24" N, 15°22'8" W), we deployed eight

floating *in situ* mesocosms, which are the shorter equivalents of the KOSMOS mesocosm design (Riebesell et al., 2013). They are 2 m in diameter, 4 m long and possess a 1 mm thick bag made of transparent polyurethane. Their cylindrical main body tapers off into a conical sediment trap at the bottom, from which sinking material can regularly be sampled. On the 6th of September (experimental day 0) they were filled simultaneously with ~8 m^3 of oligotrophic water from outside the harbor. During the filling, a 3 mm mesh at the water inlet kept larger organisms from entering the mesocosms.

During the 35 day-long experiment, the enclosed plankton communities were subjected to recurring additions of nutrient-rich deep water. The water was collected west of Gran Canaria at ~120-160 m depth at two different locations (27°52'16" N, 15° 18'48" W and 28°00'01"N, 15°20'11"W). Before the deep water addition to the mesocosms, inorganic nutrients were added to reach our desired nutrient levels. Thereby, C, N and P were supplied at Redfield ratios (C:N:P = 106:16:1), reaching nitrate concentrations of 30 µmol L^{-1} with corresponding 1.9 µmol L^{-1} of phosphate and 199 µmol L^{-1} of additional dissolved inorganic carbon. Nitrate thereby served as the reference for the Si:N treatment. Silicic acid ($Si(OH)_4$) was added in different amounts (between 2 and 40 µmol L^{-1}, Figure 1A) to achieve the specific treatment levels. These were chosen to mimic the different stoichiometries of potential source waters from different locations (Sarmiento et al., 2004; Griffiths et al., 2013) and depths (Llinás et al., 1994; Sarmiento et al., 2007). The first upwelling treatment was carried out on day 6, and was repeated every other day until day 32 (Figure 1B).

Iron influences Si:N ratios in pelagic systems. Upwelled deep waters stripped of iron, for example, can limit productivity and elevate the uptake of Si relative to other nutrients by diatoms (Hutchins and Bruland, 1998; Hutchins et al., 1998; Jickells et al., 2005). Yet, given the geographic location and experimental facility, we did not control for iron in our study. Firstly, iron inputs are plentiful around Gran Canaria through atmospheric dust deposition (López-García et al., 2021) and resuspension from shelf sediments. Secondly, contamination via measurement devices generally causes relatively high dissolved iron (dFe) concentrations inside mesocosms. In another one of our studies at the same location and in the same season that deployed the same set of mesocosms, dFe ranged from 0.54 to 4.15 nM (pers. comm. Magdalena Santana). The same mesocosm system off the coast of Peru ranged from 3.1 to 17.8 nM dFe (Bach et al., 2020). These dFe concentrations are substantially higher than in Atlantic Ocean surface waters (0 to ~1.0 nM, Sarthou et al., 2003; Bergquist and Boyle, 2006; Rijkenberg et al., 2014; Hatta et al., 2015; Tonnard et al., 2020). Iron was likely also abundant in our experiment and not limiting diatoms.

To maintain the pelagic quality of the enclosed ecosystems, the mesocosm bags were cleaned regularly using a ring-shaped wiper or by divers equipped with brushes to prevent the attachment of fouling organisms (Figure 1B). For more information on the experimental setup, the mesocosm maintenance and the deep water collection see Goldenberg et al. (2022).

The small pelagic silverside *Atherina presbyter* was introduced to each mesocosm as early juvenile (n = 45, length = 17 mm) and young larvae (n = 36, length = 9 mm) on day 15. They were removed from the mesocosms on day 21 to assess survival and growth. The mesozooplankton community was depleted by the fish and could not recover. Given that all mesocosms were affected equally, this restructuring of the food web unlikely biased our Si:N treatment. Before fish introduction, there had already been a pronounced mismatch between phyto- and mesozooplankton in all mesocosms, as primary producers with short generation times rapidly outgrew their grazers (Goldenberg, unpublished data). During the experimental period organic matter export was hence

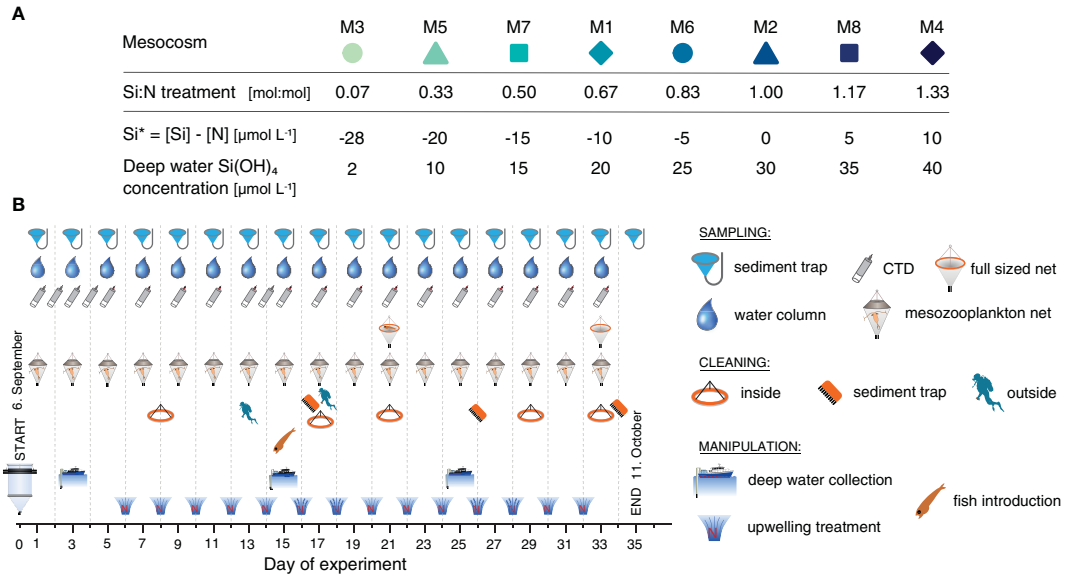

FIGURE 1
Si:N treatment per mesocosm **(A)** and experimental timeline with sampling, cleaning and manipulation schedule **(B)**.

based on a truncated food web, in which phytoplankton could grow unchecked by mesozooplankton grazers.

2.2 Sampling procedure

Water column and sediment trap samples were taken every to every second experimental day for the analysis of various biogeochemical and ecological parameters. The samples were analyzed in the nearby laboratory facilities of the Plataforma Oceánica de Canarias (PLOCAN) and the University of Las Palmas de Gran Canaria (ULPGC). Integrated water column samples were taken using submersible, 2.5 m long plastic tubes (Ø 53 mm, 5.13 L). They were transferred to 10 L carboys and stored dark and cold until arrival in the laboratory. There, they were subsampled for the analysis of phytoplankton abundances, composition and biomass and concentrations of particulate biogenic matter. Mesozooplankton samples were taken with tubes and nets (Apstein Ø 17 cm, 56.7 L, 55 µm mesh size). Sedimented material was sampled every second day through the hose attached to the sediment traps by means of a manual vacuum pump (<0.3 bar). It was collected in 5 L glass bottles (Schott Scandinavia, Denmark) and stored dark until further processing. In the lab, the sediment bottles were gently rotated to homogenize the material, and subsequently subsampled for measurements of sinking velocity and remineralization rates. The remainder of the material was prepared for the analysis of particulate biogenic matter, including particulate organic carbon, nitrogen and phosphorus (POC, PON, POP), total particulate carbon (TPC) and biogenic silica (BSi).

2.3 Sample processing and measurement

2.3.1 Sediment trap material

After subsampling, the settled biogenic matter had to be separated from sea water (see Boxhammer et al., 2016). 3 mol L^{-1} of ferric chloride ($FeCl_3$) were added to the sediment bottles to make the material flocculate, followed by 3 mol L^{-1} of NaOH as a pH buffer, after which the bottles were left alone for 1 h to let the material settle. Subsequently, the supernatant sea water was carefully decanted. The sediment suspension was then centrifuged at ~5,200 *g* for 10 min in a 6–16KS centrifuge (Sigma Laborzentrifugen, Germany), and then again at ~5,000 *g* for 10 min in a 3K12 centrifuge (Sigma). This yielded sediment pellets, which were frozen at –20°C and transported to Kiel, where their elemental composition was analyzed. In Kiel, the pellets were freed of any leftover moisture by freeze-drying and ground in a cell mill (Edmund Bühler, Germany), to obtain fine and homogeneous sediment powder. This powder was then weighed and subsequently subsampled for TPC, POC, PON, BSi and POP measurements.

Subsamples for TPC and PON were transferred into tin cups (8 × 8 × 15 mm, LabNeed, Germany) and measured after Sharp (1974) in duplicates on a Euro EA-CN analyzer (HEKAtech, Germany). POC subsamples were fumed with 1 mol L^{-1} HCl to remove the particulate inorganic carbon (PIC) fraction and dried at 50°C overnight before they were measured similarly. The PIC content was estimated as the difference between TPC and POC. As there were no treatment effects on PIC export, this parameter is not shown in this study. Biogenic silica and particulate organic phosphorus concentrations were measured spectrophotometrically following Hansen and Koroleff (1999). The mass fluxes to the sediment trap were calculated by upscaling the measured C, N, Si and P concentrations in the subsamples to the total sample weight. The mass fluxes were then normalized to the time between sample collection (48 h) and to the mesocosm volume to obtain daily mass fluxes in µmol L^{-1} d^{-1}. The relative contribution of BSi (BSi fraction) to the total export flux as a proxy for BSi ballasting was calculated according to Bach et al. (2016).

$$BSi\ \ fraction = \frac{2.1\ \frac{g}{cm^3} * BSi}{1.06\ \frac{g}{cm^3} * POC + 2.1\ \frac{g}{cm^3} * BSi + 2.7\ \frac{g}{cm^3} * PIC} \quad (1)$$

where the daily export fluxes of BSi, POC and PIC are multiplied with their respective densities (Klaas and Archer, 2002).

2.3.2 Water column samples

The integrated water samples were analyzed for their POC, PON and total particulate carbon (TPC) concentrations. Therefore, subsamples were taken in our on-shore labs and the suspended particles were collected on pre-combusted glass fiber filters (0.7 µm, Whatman). Filters for POC and PON analyses were acidified for ~2 h with 1 mol L^{-1} HCl to remove the inorganic carbon fraction. Filters for POC/N and TPC were then dried for 24 h at 60°C in pre-combusted glass petri dishes. They were packed into tin cups and transported back to Kiel, where their carbon and nitrogen contents were measured on a CN analyzer, as described for sedimented matter above. The particulate inorganic carbon content was estimated as the difference between TPC and POC. Since we did not find consistent evidence for the presence of particulate inorganic carbon (Goldenberg et al., 2022), we pooled the TPC and POC/N filters to obtain POC and PON duplicates.

Diatom biovolume was estimated using the Utermöhl method (Edler and Elbrächter, 2010). Water samples were fixed with Lugol's iodine (final concentration of 1%) and stored inside 250 mL brown glass bottles. Subsamples were transferred to settling chambers (20–50 mL), from which cells were counted after 24 h using inverse light microscopy. A minimum of 500 phytoplankton cells per taxa were counted and identified to the lowest possible taxonomic level. Due to the high phytoplankton abundances, not all cells per subsample were counted, but a minimum of 500 cells across all taxa. The dimensions of the dominant taxa were regularly measured, and, based on average sizes, their specific biovolumes were calculated (Olenina et al., 2006). Total diatom biovolume was calculated from cell abundances and per capita biovolume.

2.3.3 Sinking velocity of sediment trap particles

In order to assess the potential transfer efficiency of sinking particles, we measured sinking velocities (SV) of particles in the 40–1000 µm size spectrum. We therefore used a video microscopy method, which was developed by Bach et al. (2012) and further reworked by Bach et al. (2019) and Baumann et al. (2021). Diluted

sediment subsamples were transferred to a sinking chamber (1 x 1 cm edge length), which was vertically mounted on a FlowCam device (Fluid Imaging Technologies, United States). Settling particles were therein recorded for 20 min at ~7 fps. Particle sinking velocities were calculated by fitting a linear model to the y-positions of multiple captures of the same particle and their respective time stamps. The calculations were carried out using the MATLAB software (version R2018b). Particles out of focus were excluded from the analysis based on the blurriness of their contour lines. Wall effects of the sinking chamber were corrected for using the equation in Ristow (1997). Because of the temperature-dependence of sinking velocity measurements (Bach et al., 2012), our laboratory was temperature-controlled and set to 22–23°C, depending on the daily *in situ* mesocosm temperatures.

Alongside sinking velocity, particle size as equivalent spherical diameter (ESD) and porosity (i.e. compactness) as a size-normalized measure for particle intensity (P_{int}) were measured. The underlying assumption of our porosity-proxy was that porous particles appear brighter (translucent) whereas more compact ones appear darker (opaque). High intensity values (i.e. brighter images) thus resulted in high porosities and vice versa. As large particles are generally more porous than small ones (Laurenceau-Cornec et al., 2020), our porosity-proxy is size-dependent, and was calculated following Bach et al. (2019):

$$P_{int} = (intensity/255)^2 * ESD \quad (2)$$

We analyzed sinking velocity and particle properties in four different particle classes: small (40–100 µm), medium (100–250 µm) and large particles (250–1000 µm), as well as the fastest 10% of sinking particles across the three size fractions. For every measurement (i.e., mesocosm X on day Y) we calculated mean sinking velocities and particle properties in each of these classes across all measured particles. As fast sinking particles are particularly important for carbon sequestration processes (see Section 4.1) and since we detected the strongest treatment effects in this particle class, we mainly focus on the fast sinking particle class in our analysis. Note that size fractions that included fewer than five particles were removed from the analysis, which encompassed the 250–1000 µm size fraction of M4 on days 5 and 21. This threshold shall prevent outliers based on a handful of data points to drastically affect statistical data analysis.

2.3.4 Remineralization rates of sinking particles

The other factor that determines the transfer efficiency of particulate matter exported via the biological carbon pump is its remineralization rate. The higher it is, the lower the efficiency of carbon transfer to depth. Here, we measured the carbon-specific remineralization rate of sedimented material every 4 days via the oxygen depletion rate in dark-incubated sediment. Therefore, seven 330 mL glass bottles (Schott) were sampled headspace-free from the water column of each mesocosm. Four of these were used as replicates and three as controls ((4 + 3) bottles × 8 mesocosms = 56 bottles in total). They were transported dark and cool to the temperature-controlled lab (daily *in situ* temperature), where they acclimatized for 2 h in a water bath. There, between 0.5–3 mL of sediment suspension from sediment subsamples of the respective mesocosm was carefully added to the replicate bottles, while the controls were left untreated. A plastic pipette with a widened tip was used for the sediment addition to keep aggregates intact. All bottles were then incubated in darkness on a rotating plankton wheel (~1 rpm), and oxygen depletion over time was measured. O_2 measurements were carried out non-invasively on PSt3 optodes (PreSens Precision Sensing, Germany) mounted inside the bottles using a handheld optical measurement device (Fibox4 Trace, PreSens). They were automatically corrected for temperature, which was measured in a dummy bottle, and for atmospheric pressure measured by the Fibox4. Salinity was corrected for using the respective mesocosm salinity, measured by CTD casts on the respective day. The eight incubations lasted on average ~27 h, during which 5–8 O_2 measurement were carried out in intervals of 2–6 h. After the incubations the particulate matter inside the bottles was collected on pre-combusted glass fiber filters (0.7 µm, Whatman) and their POC contents analyzed similarly as for the suspended particle filters.

Carbon-specific remineralization rates (C_{remin}, d^{-1}) were calculated by dividing the O_2 depletion rate (r in µmol O_2 L^{-1} d^{-1}) of the sediment material by its measured POC content (µmol C L^{-1}) at the end of the incubation:

$$C_{remin} = \frac{(r * RQ)}{(POC + r * RQ * \Delta t)} \quad (3)$$

Thereby, RQ is the respiratory quotient (µmol C µmol O_2^{-1}), commonly regarded as 1, i.e. 1 mol CO_2 produced: 1 mol O_2 consumed (Ploug and Grossart, 2000; Iversen and Ploug, 2013; Bach et al., 2019), and the time interval between the start of the incubation and the filtration start is factored in as Δt (d). C-specific remineralization rates were calculated for both sediment-containing bottles and blank bottles with only mesocosm water. The remineralization rates of the sedimented particulate matter were calculated by correcting the rates of the sediment-containing bottles for the rates in the blank bottles.

Finally, we calculated the remineralization length scale (RLS, m) as the quotient of sinking velocity (SV, m d^{-1}) and carbon-specific remineralization rates (C_{remin}, d^{-1}). It resembles the vertical distance over which 63% of the sinking POC flux are being remineralized back to inorganic carbon (Cavan et al., 2017).

$$RLS = \frac{SV}{C_{remin}} \quad (4)$$

2.4 Data analysis

The eight mesocosms were replicates along the established Si:N artificial upwelling gradient, sampled repetitively throughout the experiment. Linear mixed effects models with random intercept were used to detect effects of the upwelled Si:N ratio and its change over time on export parameters (vertical fluxes and stoichiometries, particle sinking velocities and degradation rates). Si:N and experimental Day were employed as continuous and categorical fixed effect, respectively, and Mesocosm as random effect. The

interaction term of Si:N × Day was employed as additional fixed effect to test how the Si:N effect changed over time. This is particularly relevant for pelagic food webs, in which temporal dynamics can strongly affect ecosystem responses to environmental changes such as upwelling. To assess the effect of silicon-associated export mechanisms (e.g. BSi ballasting) on particle sinking velocity more directly, the exported Si:N ratio (i.e. exported BSi to exported PON, Figure S1) was established as continuous explanatory variable in addition to upwelled Si:N (see Tables S2F–I).

The models were fit using restricted maximum likelihood and a type III test with Satterthwaite's approximation. All data analyses were carried out with R (version 4.1.2, R Core Team, 2021; RStudio Team, 2022). For data exploration and visualization the "tidyverse" package was used (Wickham et al., 2019). Statistical testing was performed using "lme4" (Bates et al., 2015) and "lmerTest" (Kuznetsova et al., 2017) at a significance level of $\alpha = 0.05$. Normality of residuals and random effects were checked with Q-Q plots, homogeneity of variance with residuals versus fitted plots (package "performance" (Lüdecke et al., 2021). Data was transformed where necessary. In addition, the temporal development of the Si:N effect was examined. Therefore, linear regressions for each sampling day were computed and their slopes ± 95% confidence intervals plotted over time.

Based on the daily export fluxes and stoichiometric ratios (see Figures 2B–E; Figure S1), we segmented the experiment into three phases to be able to discuss our results more comprehensively: oligotrophic baseline (days 3–9), initial response (days 11–21) and long-term response (days 23–35).

3 Results

3.1 Diatom community and particulate matter export

Artificial upwelling fueled diatom growth in all mesocosms. High Si fertilization additionally accelerated bloom development during the initial growth phase (Goldenberg et al., 2022). The diatom blooms were formed mainly by the chain-forming *Leptocylindrus* and the pennate *Pseudo-nitzschia* genera. Both are ubiquitous (Trainer et al., 2012; Ajani et al., 2021) and *Leptocylindrus* has often been abundant in mesocosm experiments (Roberts, 2003; Taucher et al., 2018b; Ortiz et al., 2022). *Pseudo-nitzschia* is known to produce the toxin domoic acid, of which we found no relevant concentrations in our experiment. Throughout the treatment application, diatom abundances and total biovolume were higher under Si-rich upwelling than under Si scarcity (Figure 2A), indicating that abundant Si promoted plenty of building material for frustules.

The diatom blooms caused increased export of freshly produced particulate matter to the sediment traps (Figure 2B). This material was characterized by elevated C:N ratios compared to pre-upwelling conditions (Figure 2C). Higher upwelled Si:N ratios further enhanced both particulate organic carbon export and exported C:N ratios during the initial treatment response phase (days 11–21). Actively managing silicon to nutrient ratios thus affected the export of organically bound carbon during the system's adjustment to artificial upwelling.

Increased export fluxes as a response to upwelling and to high Si:N ratios were primarily observed for carbon, nitrogen and silicon pools (see Figures 2B, D; Figure S1). Particulate organic carbon and nitrogen export increased on average 3- and 2.5-fold from the pre-treatment (days 3–9) to the initial response phase (days 11–21), respectively, while biogenic silica export increased 1.7-fold. In contrast, the export of total particulate phosphorus did not increase (Figure S1). The Si:N treatment was reflected most clearly by the biogenic silica flux, the BSi fraction of the total flux (Figures 2D–E) and the exported Si:N ratio during the initial and long-term response phases (Figure S1). Si-rich upwelling did thus not only cause a higher BSi flux, but also increased the BSi ballasting of sinking particles (Table S1). Both effects persisted throughout the initial and long-term response phases. In contrast, the positive Si:N effect on POC export and exported C:N ratios disappeared during the long-term response phase. The peak in the export flux parameters on day 19 (Figures 2B, D; Figure S1) was likely a consequence of the cleaning of the inside mesocosm walls and the sediment traps on day 17 (compare Figure 1; Figures 2B, D). This removed the biofilm and fouling organisms from the vertical mesocosm walls and brushed particles off the walls of the funnel-shaped sediment trap into the collection container.

3.2 Sinking particle characteristics

The nutrient composition in the upwelled water affected the properties of sinking particles. Surprisingly, high Si:N in upwelled waters temporarily decreased sinking velocity and size of the fastest sinking particles (Figures 3B–F). The effect was similar, although slightly weaker, for sinking velocities classified by particle size (Figure S2; Table S2). These effects occurred mainly between days 17 to 25. During this time, the relationship between the exported Si:N ratio and sinking velocity (or particle size) yielded similar results (Figures 3D, H; Table S2F-I). This shows that a high proportion of biogenic silica ballast correlated with smaller sizes and lower sinking speeds of the fast sinking particle fraction. Moreover, the reduced sinking speeds in the high Si:N treatments were not only associated with smaller sizes, but possibly also with lower particle porosities (Figure 3G).

The remineralization rates of sinking particulate matter increased when freshly produced material sank to the sediment traps at the onset of the upwelling treatment and subsequently decreased again towards the end of the experiment (Figure 3A). In contrast to sinking velocities, remineralization rates were however not affected by the upwelled Si:N ratio (Table S2), except for day 15, on which there was a small positive effect.

We found that high sinking velocities of fast sinking particles were associated with low to moderate diatom presence, whereas high diatom abundances did seemingly not allow for fast sinking (Figure 4A). Likewise, fast sinking particles and high C:N ratios did not co-occur while the Si:N treatment effect was strongest (Figure 3E; Figure 4B). Hence, the exported particles in between days 17 and 25 were either fast sinking or carbon-rich, but not both. Finally, only a part of the over-consumed carbon under high Si:N upwelling was exported. Under high Si:N, the C:N ratios of

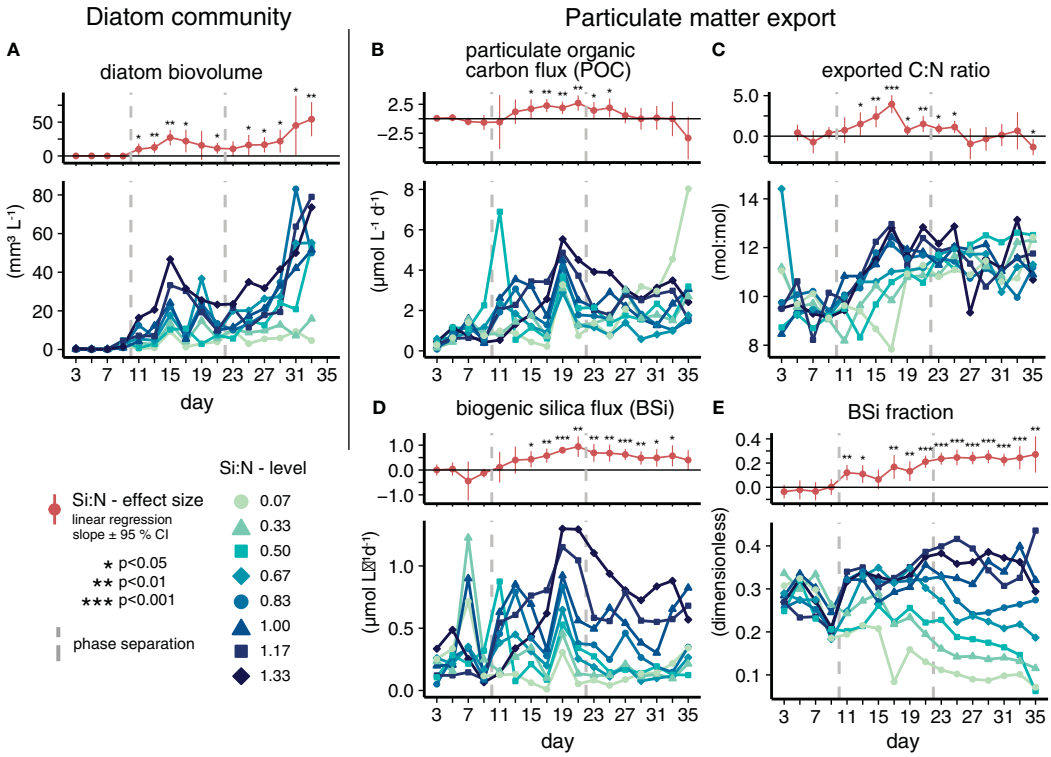

FIGURE 2
Suspended diatoms **(A)** and particulate matter export **(B–E)** under varying Si:N of upwelled water. The detailed development of individual mesocosms (lower subpanels) and the effect of the Si:N treatment across all 8 mesocosms on each day (upper subpanels) are provided. Units are valid for both panels.

suspended particles were very high (~10–17.5 mol:mol), however, the exported matter was carbon-depleted relative to the suspended material (Figure 4C). This indicates a retention of C in the water column. In contrast, under low Si:N, suspended particle C:N ratios were relatively low (~5–12 mol:mol), and exported matter was carbon-enriched compared to the suspended material (retention of N in the water column, Figure 4C). This indicates that the additionally taken-up carbon under high Si:N was partly retained as suspended POC (i.e. non-sinking particles) in the water column instead of being channeled into export production. The amount of silicon relative to nitrogen in artificially upwelled water thus affected export-related parameters in counteracting ways.

4 Discussion

4.1 Counteracting effects of Si:N upwelling

POC export and associated C:N ratios increased after the onset of artificial upwelling. This finding is similar to an earlier artificial upwelling mesocosm study (Baumann et al., 2021). The Si:N composition in the artificially upwelled water had positive effects on the magnitude of the export flux as well as its C:N stoichiometry, both of which is beneficial for potential carbon sequestration. This was caused by higher diatom abundances and elevated C:N ratios of suspended particles during the initial response phase of Si-rich upwelling (Goldenberg et al., 2022). Upwelled Si:N further had a lasting positive effect on biogenic silica export and the relative contribution of BSi ballast to sedimented matter. High upwelled Si:N ratios thus promoted several key factors which should in theory favor the carbon sequestration potential.

Curiously though, the more than 3-fold increase in BSi ballast under Si-rich upwelling did not result in higher particle sinking velocities. On the contrary, particles under enhanced BSi ballasting in the highest Si:N treatment temporarily sank only about half as fast as particles in the lowest Si:N treatment. The reason for this was most likely that particles under Si-replete conditions were ~100 µm smaller than the ones experiencing Si-scarce upwelling. As sinking velocity is usually positively affected by particle size for similar particle types (Cael et al., 2021), the decreased particle size apparently outweighed the positive effect of enhanced BSi ballast. Although we found this negative Si:N effect on sinking velocities for almost all considered particle size classes, it was most prominent for those particles that sank fastest (Table S2). These fast sinking particles can be considered the most important contributor to the biological pump as they reach the sequestration depth most rapidly and spend the least amount of time in the mesopelagic zone, where the majority of remineralization occurs (Mayor et al., 2014; García-Martín et al., 2021). Additionally, they are often large and hence incorporate high amounts of organic carbon. The speed with which the fastest particles sink is thus an important predictor for carbon sequestration processes (Riley et al., 2012).

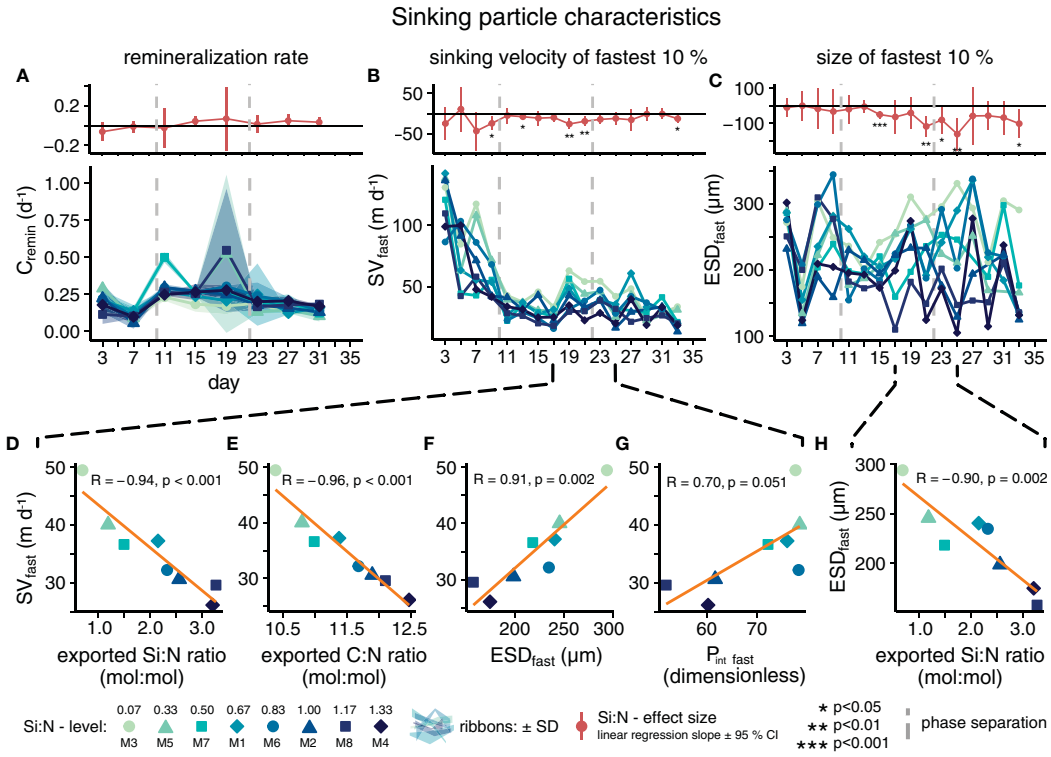

FIGURE 3
Development of sinking particle characteristics over time with daily Si:N effect sizes **(A–C)** and relationship between key export parameters **(D–H)**. Particle sinking velocities, sizes and porosities in **(B–H)** are means of the fastest 10% of sinking particles **(B–F)**. **(D–H)** incorporate mean data from days 17 to 25, the period of strongest, negative Si:N effects.

Our *ex situ* sinking velocity measurements may have been affected by our sediment sampling and processing: Both aggregation and disaggregation processes might thereby have altered the particle size distribution and sinking velocities to some (unknown) extent. As all samples were handled equally, they might have all been affected similarly by such systematical methodological artefacts. However, since the quality of sinking particles varied across Si:N treatments, it is possible that the handling influenced samples in different ways. For instance, more fragile aggregates might have been affected more strongly than sturdier ones. Thus, we cannot exclude the possibility that the negative Si:N effect on particle size was influenced by sample handling, i.e. that samples

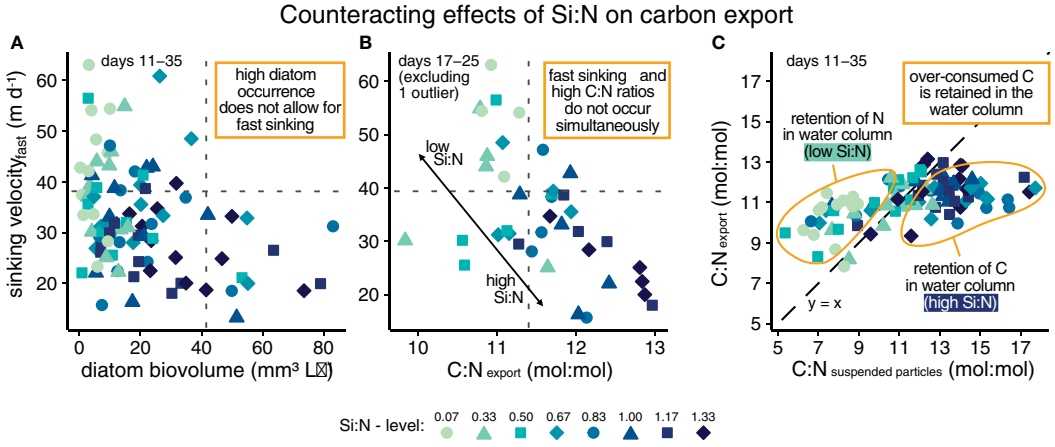

FIGURE 4
Summary figure displaying the counteracting effects of upwelled Si:N on export related parameters **(A-C)**. The dashed line in **(C)** indicates no change in C:N ratios from suspended to exported particles. Note that the data point M3 on day 17 was excluded as an outlier (exported C:N ratio: 7.8 mol: mol, sinking velocity of fastest 10%: 33.4 m d^{-1}).

under high Si:N were more fragile and experienced more disaggregation than under Si scarcity.

Another counterintuitive finding was the positive – albeit borderline insignificant – correlation between sinking velocity and particle porosity at the end of the initial response phase (Figure 3G). Theoretically, porosity should negatively affect a particle's sinking velocity by lowering its density (Laurenceau-Cornec et al., 2020). We assume that the reason for our contradictory result is the size-dependency of porosity (see Equation (2)). Very porous particles were also large and therefore likely sank more quickly (Alldredge and Gotschalk, 1988; Xiang et al., 2022). Increasing size might have accelerated particles despite decreasing BSi ballast and increasing porosity.

The question remains why increased Si availability drove smaller sizes and lower sinking velocities during the end of the adjustment phase. The slower sinking could possibly be explained by elevated exudation of transparent exopolymer particles (TEP) under Si-rich upwelling. TEP can act as "biological glue" and promote aggregation, but it can also retain suspended matter in the surface layer due to its positive buoyancy (Mari et al., 2017). During an earlier mesocosm campaign in the Canary island region, TEP increased sharply following a simulated artificial upwelling event (Taucher et al., 2018a), and was provided as the reason for the decrease of particle sinking velocities (Bach et al., 2019). Whilst we did not measure TEP in the current study, the association of high C:N ratios with slow sinking velocities hint at its presence . The conditions for its exudation were favorable under high Si:N upwelling. Firstly, nutrients were quickly depleted following each deep water addition (Goldenberg et al., 2022), resulting in regular nutrient limitation that encourages TEP exudation (Obernosterer and Herndl, 1995; Mari et al., 2017). Secondly, diatoms that are typical TEP producers under post-bloom conditions (Taucher et al., 2015; Taucher et al., 2018a) were more abundant under Si-rich upwelling.

TEP exudation could explain why carbon-rich particulate matter sank slowly under high upwelled Si:N. However, one would concurrently expect increased aggregation and hence larger particles. Yet, we observed the opposite. Figure 5 shows representative images of a subsample of sedimented material aligned along the Si:N upwelling gradient. Under Si scarcity particles were large and contrasted strongly with the background, whereas under abundant Si, single particles were smaller and hardly distinguishable. Potentially, TEP exuded under high Si:N was more numerous but less sticky, leading to smaller, more slowly sinking aggregates. Another possibility is that sampling procedures broke apart aggregates under high upwelled Si more easily. In the end, these explanation attempts remain speculative and the mechanism for the negative Si:N effect on sinking velocities and particle sizes cannot be fully disclosed.

Summing up, enhancing the proportion of Si in artificially upwelled water increased BSi ballasting of sinking particles but also resulted in a rather counter-intuitive decrease in particle sizes and ultimately lower sinking velocities. Furthermore, remineralization of sinking particles did not change with upwelled Si:N ratio, indicating that BSi apparently did not shield organic matter from respiration (Boyd and Trull, 2007). High BSi ballasting did thus not go hand in hand with beneficial particle properties for transfer efficiency. When considering the correlations between BSi and POC fluxes in the deep ocean (Klaas and Archer, 2002), our findings suggest that in the surface ocean the positive effects of BSi ballasting on POC fluxes are superimposed by other drivers. For example, the enhanced formation of positively buoyant TEP could exert a negative control on sinking velocities (Azetsu-Scott and Passow, 2004) and retain carbon-rich material in the surface (Mari et al., 2017). As particles sink through the epi- and mesopelagic zones, the preferential remineralization of organic material, including TEP, might leave a higher fraction of BSi behind and could thus be the reason for the observed correlations between POC and BSi at depth (Sanders et al., 2010). It is important

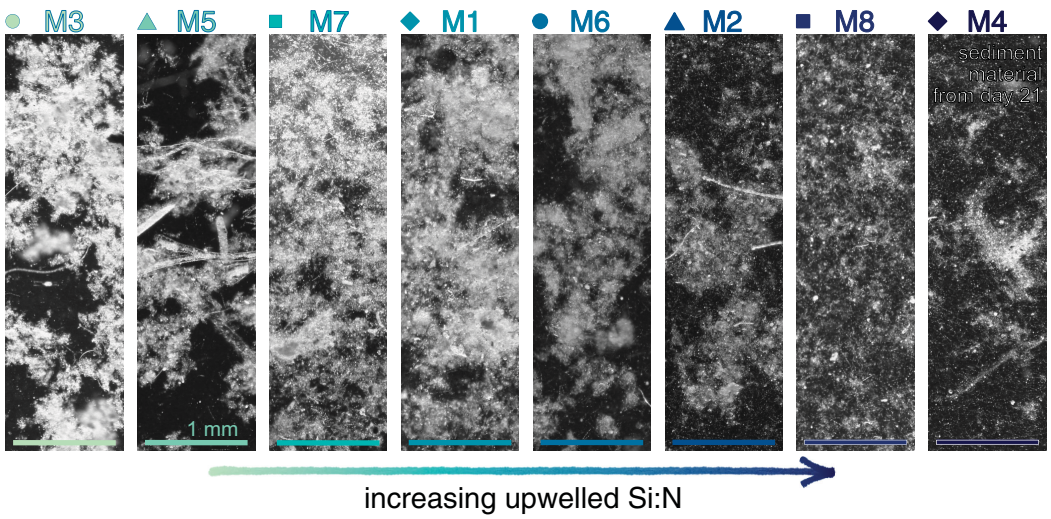

FIGURE 5
Material sampled from the sediment trap of each mesocosm on day 21. Pictures were taken on a stereo microscope (Stemi 305, ZEISS) and are displayed on a greyscale to emphasize structural differences.

to note that due to the strong mismatch between phytoplankton and mesozooplankton grazers during this experiment, the latter did not play a major role for export production via e.g. repackaging and fecal pellet production. Therefore, our findings on how the upwelled Si:N ratio affected export parameters may not apply to systems in which mesozooplankton exerts a strong top-down control. Under such conditions, reworking of suspended and sinking particles might lead to different particle types sinking, possibly promoting a BSi ballast effect.

4.2 Implications for artificial upwelling as negative emission technology

The various Si:N effects on export parameters in our study were of counteracting nature. Some imply an increased potential for carbon sequestration and thus carbon removal from the atmosphere, others are unfavorable in that aspect (Figure 6). In the following, we will discuss the relative importance of our findings in respect to the carbon removal potential of artificial upwelling.

The key Si:N effects concerning the carbon sequestration potential are the positive effects on POC flux, exported matter C:N ratios and BSi ballasting on the one side, and the negative effects on sinking velocities and the relative difference between suspended and exported C:N ratios on the other (Figure 6). Si-replete conditions temporarily caused more material to be exported from the surface and positively affected the C:N ratio of exported matter, both of which strengthens the biological carbon pump. However, the C:N effect was potentially buffered by the retention of parts of the over-consumed carbon as suspended POC in the water column, and additionally, sinking velocities decreased, which hampered the potential for efficient carbon transfer to depth.

The question is whether the increased POC flux and elevated C:N ratios, or the decreased sinking velocities would have had a larger impact on the realized carbon deep export. The remineralization length scale (RLS), a proxy for the POC transfer efficiency, helps to get an understanding of the relative importance of flux quantity versus quality. Figure 7 shows surface POC fluxes, the RLS and theoretical attenuated POC fluxes at the respective RLS depth for the lowest and highest Si:N treatment on day 21. On this day, there were pronounced and rather linear Si:N effects, making this comparison representative of the range of upwelled Si:N ratios tested here. Due to the 2.5-fold higher particle sinking velocities under low Si:N, the transfer of organic carbon to depth would have likely been more efficient in the lowest compared to the highest treatment (RLS depth more than 2-fold deeper). Nonetheless, the 6-fold higher POC flux under the highest Si availability would have probably led to more POC sinking out of the euphotic zone (50–100 m depth) in this treatment. We can, however, not say whether the enhanced flux attenuation under high Si:N would ultimately lead to less POC reaching the deep ocean than under Si-scarcity. The flux and sinking velocity measurements herein stem from the very surface layer (4 m depth), and it is complicated to predict the fate of sinking matter fluxes to greater depths. Even for approximations, a sophisticated flux attenuation model would be needed, which is beyond the scope of this study. We hence emphasize the importance of incorporating our experimental findings into biogeochemical models. This would help to resolve the relative importance of counteracting effects of artificial upwelling as a carbon removal technique.

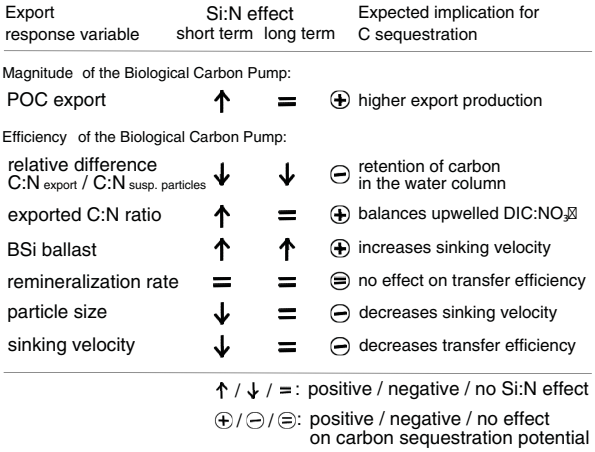

FIGURE 6
Summary of Si:N effects under artificial upwelling on export-related parameters and their implications for the carbon sequestration potential. Short-term (initial response phase, days 11–21) and long-term (long-term response phase, days 23–35) effects are displayed.

When discussing the implications of our results, it is important to differentiate between short and long term effects. The observed short term Si:N effects carry more weight for stationary artificial upwelling applications, which result in one-time fertilization of water patches, e.g. a moored wave pump (Liu et al., 1999; Fan, 2016). Also the remineralization rates, which increased after the onset of artificial upwelling, subsequently decreased again towards the end of the experiment, and thus only temporarily hampered the efficiency of particle transfer. The long-term effects are more important regarding the application of drifting artificial upwelling devices, which fertilize the same patch of water over longer time periods. Concerning recurring upwelling, most of the Si:N effects are thus not crucial, and instead the benefit of increased POC fluxes and enhanced sinking matter C:N ratios would come into play. Those elevated carbon to nutrient ratios would, however, be buffered under Si-rich upwelling by the retention of over-consumed carbon as suspended POC in the water column.

In summary, artificial upwelling enhanced surface ocean POC fluxes and associated C:N ratios, and did so on the time scale of multiple weeks. Additionally, the upwelled Si:N ratio temporarily enhanced carbon assimilation and consequently the POC flux and exported matter C:N ratios. However, the over-consumed carbon was partly retained in the water column, possibly due to the enhanced formation of positively buoyant TEP under high diatom abundances. Furthermore, although Si-rich upwelling enhanced BSi ballasting manifold, changes in particle properties led to temporarily decreased sinking velocities and hence less efficient particle export. Actively managing Si availability under artificial upwelling thus caused conflicting changes to export-relevant system properties of the surface ocean. This indicates that in a real world application it could be challenging to find the

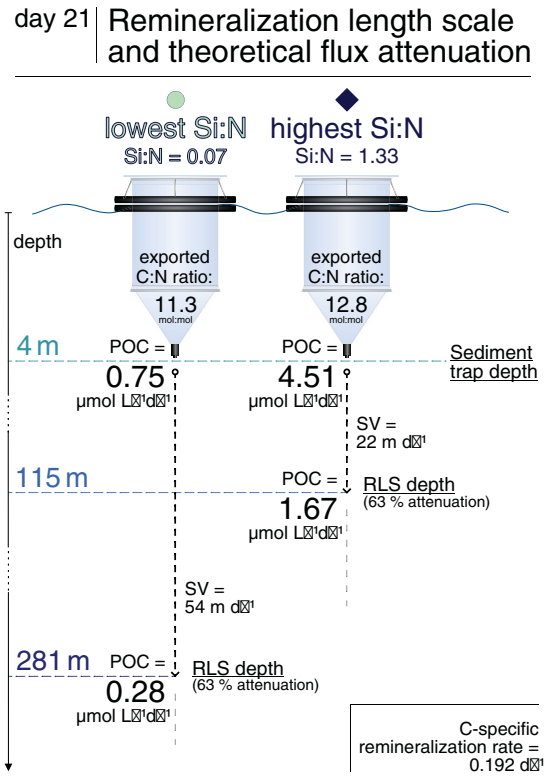

FIGURE 7
Remineralization length scale (RLS) and resulting flux attenuation for the highest and lowest Si:N treatments on day 21. RLSs were calculated from sinking velocities (SV) of the fastest sinking particles on day 21 and remineralization rates from day 23 averaged across mesocosms. See Figure S2 for further RLS data.

right balance between favorable and unfavorable effects on carbon sequestration. In a next step, modelling approaches could help to resolve the relative importance of these findings by incorporating them into POC flux attenuation simulations. Ultimately, artificial upwelling research will need open ocean trials with sophisticated deep flux monitoring in order to verify previous results and accurately assess its carbon sequestration potential.

Data availability statement

The datasets presented in this study can be found in online repositories. The names of the repository/repositories and accession number(s) can be found below: PANGAEA data repository (https://doi.org/10.1594/PANGAEA.956371).

Author contributions

Experimental concept and design: UR, JT, SG, MF-M. Execution of the experiment: MB, SG, JT, MF-M, JO and UR. Data analysis: MB, SG, JH. Manuscript writing: MB with input from all co-authors. All authors contributed to the article and approved the submitted version.

Funding

This study was conducted in the framework of the Ocean Artificial Upwelling (Ocean artUp) and the Road Testing Ocean Artificial Upwelling (Test-ArtUp) projects. The former was funded by an Advanced Grant of the European Research Council, the latter by the German Marine Research Alliance (DAM). The EU project AQUACOSM and the project TRIATLAS (AMD-817578-5) from the European Union's Horizon 2020 provided additional Transnational Access funds.

Acknowledgments

We thank the Oceanic Platform of the Canary Islands (Plataforma Oceánica de Canarias, PLOCAN) and the Marine Science and Technology Park (Parque Cientiífico Tecnoloìgico Marino, PCTM) from the University of Las Palmas (Universidad de Las Palmas de Gran Canaria, ULPGC) for providing research facilities as well as logistical and technical support before, during and after this experiment. We are grateful to the staff and students from the KOSMOS team (GEOMAR) and the ULPGC biological oceanographers for organizing and carrying out the experiment. Finally, we thank Greta Wunderlich, Jana Meyer and Levka Hansen for their contribution to data analysis and data exchange.

Conflict of interest

The authors declare that the research was conducted in the absence of any commercial or financial relationships that could be construed as a potential conflict of interest.

Publisher's note

Supplementary material

The Supplementary Material for this article can be found online at: https://www.frontiersin.org/articles/10.3389/fmars.2023.1181351/full#supplementary-material

SUPPLEMENTARY FIGURE 1
Particulate matter export flux (daily flux, cumulative flux and elemental ratios) and daily Si:N effect sizes. Effect sizes of exported C:N and exported Si:N ratios on day 3 were removed in order to improve readability (-1.64 ± 4.15 and -4.55 ± 9.14 mol mol^{-1}, respectively).

SUPPLEMENTARY FIGURE 2
Sinking velocities for different size fractions of the 40–1000 µm size spectrum and remineralization length scale (RLS) including daily Si:N effect sizes. RLS was calculated by dividing velocities of the fastest 10% of sinking

particles (SV_{fast}) by particle remineralization rates (C_{remin}) and is limited to the days for which there are remineralization rate measurements.

SUPPLEMENTARY TABLE 1
Linear mixed models showing the effects of artificial upwelling on particulate matter flux and stoichiometries. Si:N, Day (day 11–33) and Si:N × Day were deployed as fixed effects and Mesocosm as random effect. Significant fixed effects to be interpreted are displayed in bold. MS: mean squares; df_{Num} and df_{Den}: numerator and denominator degrees of freedom; $R^2_{marginal}$: proportion of variation explained by all fixed effects

SUPPLEMENTARY TABLE 2
(A–E): Linear mixed models showing the effects of artificial upwelling on sinking velocities and carbon-specific remineralization rate. **(F-I)**: Linear mixed models showing the relationship between sinking velocities and the Si:N ratio of the particulate export flux (BSi : PON). Si:N (or exported Si:N ratio for **(F-I)**), Day (day 11–33) and Si:N × Day were deployed as fixed effects and Mesocosm as random effect. Significant fixed effects to be interpreted are displayed in bold. MS: mean squares; df_{Num} and df_{Den}: numerator and denominator degrees of freedom; $R^2_{marginal}$: proportion of variation explained by all fixed effects

References

Ajani, P. A., Petrou, K., Larsson, M. E., Nielsen, D. A., Burke, J., and Murray, S. A. (2021). Phenotypic trait variability as an indication of adaptive capacity in a cosmopolitan marine diatom. *Environ. Microbiol.* 23, 207–223. doi: 10.1111/1462-2920.15294

Alldredge, A. L., and Gotschalk, C. (1988). In situ settling behavior of marine snow. *Limnol. Oceanogr.* 33, 339–351. doi: 10.4319/lo.1988.33.3.0339

Allen, J. T., Brown, L., Sanders, R., Mark Moore, C., Mustard, A., Fielding, S., et al. (2005). Diatom carbon export enhanced by silicate upwelling in the northeast Atlantic. *Nature* 437, 728–732. doi: 10.1038/nature03948

Armstrong, R. A., Lee, C., Hedges, J. I., Honjo, S., and Wakeham, S. G. (2002). A new, mechanistic model for organic carbon fluxes in the ocean based on the quantitative association of POC with ballast minerals. *Deep. Sea. Res. Part II.: Topical. Stud. Oceanogr.* 49, 219–236 doi: 10.1016/s0967-0645(01)00101-1

Armstrong, R. A., Peterson, M. L., Lee, C., and Wakeham, S. G. (2009). Settling velocity spectra and the ballast ratio hypothesis. *Deep. Sea. Res. Part II.: Topical. Stud. Oceanogr.* 56, 1470–1478. doi: 10.1016/j.dsr2.2008.11.032

Azetsu-Scott, K., and Passow, U. (2004). Ascending marine particles: significance of transparent exopolymer particles (TEP) in the upper ocean. *Limnol. Oceanogr.* 49, 741–748. doi: 10.4319/lo.2004.49.3.0741

Bach, L. T., Boxhammer, T., Larsen, A., Hildebrandt, N., Schulz, K. G., and Riebesell, U. (2016). Influence of plankton community structure on the sinking velocity of marine aggregates: sinking velocity of marine aggregates. *Global Biogeochem. Cycles.* 30, 1145–1165. doi: 10.1002/2016GB005372

Bach, L. T., Paul, A. J., Boxhammer, T., von der Esch, E., Graco, M., Schulz, K. G., et al. (2020). Factors controlling plankton community production, export flux, and particulate matter stoichiometry in the coastal upwelling system off Peru. *Biogeosciences* 17, 4831–4852. doi: 10.5194/bg-17-4831-2020

Bach, L. T., Riebesell, U., Sett, S., Febiri, S., Rzepka, P., and Schulz, K. G. (2012). An approach for particle sinking velocity measurements in the 3–400 µm size range and considerations on the effect of temperature on sinking rates. *Mar. Biol.* 159, 1853–1864. doi: 10.1007/s00227-012-1945-2

Bach, L. T., Stange, P., Taucher, J., Achterberg, E. P., Algueró-Muñiz, M., Horn, H., et al. (2019). The influence of plankton community structure on sinking velocity and remineralization rate of marine aggregates. *Global Biogeochem. Cycles.* 33, 971–994. doi: 10.1029/2019GB006256

Bates, D., Mächler, M., Bolker, B., and Walker, S. (2015). Fitting linear mixed-effects models using lme4. *J. Stat. Software.* 67, 1–48. doi: 10.18637/jss.v067.i01

Baumann, M., Taucher, J., Paul, A. J., Heinemann, M., Vanharanta, M., Bach, L. T., et al. (2021). Effect of intensity and mode of artificial upwelling on particle flux and carbon export. *Front. Mar. Sci.* 8. doi: 10.3389/fmars.2021.742142

Bergquist, B. A., and Boyle, E. A. (2006). Dissolved iron in the tropical and subtropical Atlantic ocean. *Global Biogeochem. Cycles.* 20, n/a–n/a. doi: 10.1029/2005GB002505

Boxhammer, T., Bach, L. T., Czerny, J., and Riebesell, U. (2016). Technical note: sampling and processing of mesocosm sediment trap material for quantitative biogeochemical analysis. *Biogeosciences* 13, 2849–2858. doi: 10.5194/bg-13-2849-2016

Boyd, P. W., and Trull, T. W. (2007). Understanding the export of biogenic particles in oceanic waters: is there consensus? *Prog. Oceanogr.* 72, 276–312. doi: 10.1016/j.pocean.2006.10.007

Cael, B. B., Cavan, E. L., and Britten, G. L. (2021). Reconciling the size-dependence of marine particle sinking speed. *Geophys. Res. Lett.* 48. doi: 10.1029/2020GL091771

Cavan, E. L., Trimmer, M., Shelley, F., and Sanders, R. (2017). Remineralization of particulate organic carbon in an ocean oxygen minimum zone. *Nat. Commun.* 8, 14847. doi: 10.1038/ncomms14847

Coale, K. H., Johnson, K. S., Chavez, F. P., Buesseler, K. O., Barber, R. T., Brzezinski, M. A., et al. (2004). Southern ocean iron enrichment experiment: carbon cycling in high- and low-Si waters. *Science* 304, 408–414. doi: 10.1126/science.1089778

Dugdale, R. C., and Wilkerson, F. P. (1998). Silicate regulation of new production in the equatorial pacific upwelling. *Nature* 391, 270–273. doi: 10.1038/34630

Edler, L., and Elbrächter, M. (2010). *The utermöhl method for quantitative phytoplankton analysis, in: microscopic and molecular methods for quantitative phytoplankton analysis* Vol. 55, 13–20 (Paris: UNESCO).

Fan, W. (2016). Experimental study on the performance of a wave pump for artificial upwelling. *Ocean. Eng.* 10. doi: 10.1016/j.oceaneng.2015.12.056

Field, C. B., Behrenfeld, M. J., Randerson, J. T., and Falkowski, P. (1998). Primary production of the biosphere: integrating terrestrial and oceanic components. *Science* 281, 237–240. doi: 10.1126/science.281.5374.237

García-Martín, E. E., Davidson, K., Davis, C. E., Mahaffey, C., McNeill, S., Purdie, D. A., et al. (2021). Low contribution of the fast-sinking particle fraction to total plankton metabolism in a temperate shelf Sea. *Global Biogeochem. Cycles.* 35. doi: 10.1029/2021GB007015

Goldenberg, S. U., Taucher, J., Fernández-Méndez, M., Ludwig, A., Arístegui, J., Baumann, M., et al. (2022). Nutrient composition (Si:N) as driver of plankton communities during artificial upwelling. *Front. Mar. Sci.* 9. doi: 10.3389/fmars.2022.1015188

Griffiths, J. D., Barker, S., Hendry, K. R., Thornalley, D. J. R., van de Flierdt, T., Hall, I. R., et al. (2013). Evidence of silicic acid leakage to the tropical Atlantic via Antarctic intermediate water during marine isotope stage 4. *Paleoceanography* 28, 307–318. doi: 10.1002/palo.20030

Guidi, L., Stemmann, L., Jackson, G. A., Ibanez, F., Claustre, H., Legendre, L., et al. (2009). Effects of phytoplankton community on production, size, and export of large aggregates: a world-ocean analysis. *Limnol. Oceanogr.* 54, 1951–1963. doi: 10.4319/lo.2009.54.6.1951

Hansen, H. P., and Koroleff, F. (1999). *Determination of nutrients, in: methods of seawater analysis, third, completely revised and extended edition* (WILEY-VCH), 159–228.

Hatta, M., Measures, C. I., Wu, J., Roshan, S., Fitzsimmons, J. N., Sedwick, P., et al. (2015). An overview of dissolved fe and Mn distributions during the 2010–2011 U.S. GEOTRACES north Atlantic cruises: GEOTRACES GA03. *Deep. Sea. Res. Part II.: Topical. Stud. Oceanogr.* 116, 117–129. doi: 10.1016/j.dsr2.2014.07.005

Henson, S. A., Lampitt, R. S., and Johns, D. (2012b). Variability in phytoplankton community structure in response to the north Atlantic oscillation and implications for organic carbon flux. *Limnol. Oceanogr.* 57, 1591–1601. doi: 10.4319/lo.2012.57.6.1591

Henson, S. A., Sanders, R., and Madsen, E. (2012a). Global patterns in efficiency of particulate organic carbon export and transfer to the deep ocean: export and transfer efficiency. *Global Biogeochem. Cycles.* 26, 34–1. doi: 10.1029/2011GB004099

Honjo, S., and Manganini, S. J. (1993). Annual biogenic particle fluxes to the interior of the north Atlantic ocean; studied at 34°N 21°W and 48°N 21°W. *Deep. Sea. Res. Part II.: Topical. Stud. Oceanogr.* 40, 587–607. doi: 10.1016/0967-0645(93)90034-K

Hutchins, D. A., and Bruland, K. W. (1998). Iron-limited diatom growth and Si:N uptake ratios in a coastal upwelling regime. *Nature* 393, 561–564. doi: 10.1038/31203

Hutchins, D. A., DiTullio, G. R., Zhang, Y., and Bruland, K. W. (1998). An iron limitation mosaic in the California upwelling regime. *Limnol. Oceanogr.* 43, 1037–1054. doi: 10.4319/lo.1998.43.6.1037

IPCC. (2018). Summary for Policymakers, in: Global warming of 1.5°C. An IPCC Special Report on the impacts of global warming of 1.5°C above pre-industrial levels and related global greenhouse gas emission pathways, in the context of strengthening the global response to the threat of climate change, sustainable development, and efforts to eradicate poverty, edited by: Masson-Delmotte,, V., Zhai,, P., Pörtner,, H.-O., Roberts,, D., Skea,, J., Shukla,, P. R., Pirani,, A., Moufouma-Okia,, W., Péan,, C., Pidcock,, R., Connors,, S., Matthews,, J. B. R., Chen,, Y., Zhou,, X., Gomis,, M. I., Lonnoy,, E., Maycock,, T., Tignor,, M., and Waterfield,, T. (Cambridge, UK: Cambridge University Press), 2018.

Iversen, M. H., and Ploug, H. (2013). Temperature effects on carbon-specific respiration rate and sinking velocity of diatom aggregates – potential implications for deep ocean export processes. *Biogeosciences* 10, 4073–4085. doi: 10.5194/bg-10-4073-2013

Jickells, T. D., An, Z. S., Andersen, K. K., Baker, A. R., Bergametti, G., Brooks, N., et al. (2005). Global iron connections between desert dust, ocean biogeochemistry, and climate. *Science* 308, 67–71. doi: 10.1126/science.1105959

Jin, X., Gruber, N., Dunne, J. P., Sarmiento, J. L., and Armstrong, R. (2006). Diagnosing the contribution of phytoplankton functional groups to the production and export of particulate organic carbon, CaCO3, and opal from global nutrient and alkalinity distributions. *Global Biogeochem. Cycles.* 2. doi: 10.1029/2005gb002532

Klaas, C., and Archer, D. (2002). Association of sinking organic matter with various types of mineral ballast in the deep sea: implications for the rain ratio. *Global Biogeochem. Cycles.* 16, 63. doi: 10.1029/2001gb001765

Kuznetsova, A., Brockhoff, P. B., and Christensen, R. H. B. (2017). lmerTest package: tests in linear mixed effects models. *J. Stat. Soft.*, 82. doi: 10.18637/jss.v082.i13

Lam, P. J., Doney, S. C., and Bishop, J. K. B. (2011). The dynamic ocean biological pump: insights from a global compilation of particulate organic carbon, $CaCO_3$, and opal concentration profiles from the mesopelagic: the dynamic ocean biological pump. *Global Biogeochem. Cycles.* 25, n/a–n/a. doi: 10.1029/2010GB003868

Laurenceau-Cornec, E. C., Le Moigne, F. A. C., Gallinari, M., Moriceau, B., Toullec, J., Iversen, M. H., et al. (2020). New guidelines for the application of stokes' models to the sinking velocity of marine aggregates. *Limnol. Oceanogr.* 65, 1264–1285. doi: 10.1002/lno.11388

Liu, C. C. K., Dai, J. J., Lin, H., and Guo, F. (1999). Hydrodynamic performance of wave-driven artificial upwelling device. *J. Eng. Mech.* 125, 728–732. doi: 10.1061/(ASCE)0733-9399(1999)125:7(728)

Llinás, O., Rodríguez de León, A., Siedler, G., and Wefer, G. (1994). *ESTOC data report 1994*, ICCM, 77.

López-García, P., Gelado-Caballero, M. D., Patey, M. D., and Hernández-Brito, J. J. (2021). Atmospheric fluxes of soluble nutrients and fe: more than three years of wet and dry deposition measurements at gran canaria (Canary islands). *Atmospheric. Environ.* 246, 118090. doi: 10.1016/j.atmosenv.2020.118090

Lüdecke, D., Ben-Shachar, M., Patil, I., Waggoner, P., and Makowski, D. (2021). Performance: an r package for assessment, comparison and testing of statistical models. *JOSS* 6, 3139. doi: 10.21105/joss.03139

Maiti, K., Charette, M. A., Buesseler, K. O., and Kahru, M. (2013). An inverse relationship between production and export efficiency in the southern ocean. *Geophys. Res. Lett.* 40, 1557–1561. doi: 10.1002/grl.50219

Mari, X., Passow, U., Migon, C., Burd, A. B., and Legendre, L. (2017). Transparent exopolymer particles: effects on carbon cycling in the ocean. *Prog. Oceanogr.* 151, 13–37. doi: 10.1016/j.pocean.2016.11.002

Mayor, D. J., Sanders, R., Giering, S. L. C., and Anderson, T. R. (2014). Microbial gardening in the ocean's twilight zone: detritivorous metazoans benefit from fragmenting, rather than ingesting, sinking detritus: fragmentation of refractory detritus by zooplankton beneath the euphotic zone stimulates the harvestable production of labile and nutritious microbial. *BioEssays* 36, 1132–1137. doi: 10.1002/bies.201400100

McDonnell, A. M. P., Boyd, P. W., and Buesseler, K. O. (2015). Effects of sinking velocities and microbial respiration rates on the attenuation of particulate carbon fluxes through the mesopelagic zone. *Global Biogeochem. Cycles.* doi: 10.1002/2014gb004935

Obernosterer, I., and Herndl, G. J. (1995). Phytoplankton extracellular release and bacterial growth: dependence on the inorganic n: p ratio. *Mar. Ecol. Prog. Ser.* 116, 247–257. doi: 10.3354/meps116247

Olenina, I., Hajdu, S., Edler, L., Andersson, A., Wasmund, N., Busch, S., et al. (2006). *Biovolumes and size-classes of phytoplankton in the Baltic Sea* (HELCOM).

Ortiz, J., Arístegui, J., Taucher, J., and Riebesell, U. (2022). Artificial upwelling in singular and recurring mode: consequences for net community production and metabolic balance. *Front. Mar. Sci.* 8, 743105 doi: 10.3389/fmars.2021.743105

Oschlies, A., Pahlow, M., Yool, A., and Matear, R. J. (2010). Climate engineering by artificial ocean upwelling: channelling the sorcerer's apprentice. *Geophys. Res. Lett.* 37. doi: 10.1029/2009GL041961

Pan, Y., Fan, W., Zhang, D., Chen, J. W., Huang, H., Liu, S., et al. (2016). Research progress in artificial upwelling and its potential environmental effects. *Sci. China Earth Sci.* 59, 236–248. doi: 10.1007/s11430-015-5195-2

Ploug, H., and Grossart, H.-P. (2000). Bacterial growth and grazing on diatom aggregates: respiratory carbon turnover as a function of aggregate size and sinking velocity. *Limnol. Oceanogr.* 45, 1467–1475. doi: 10.4319/lo.2000.45.7.1467

Puigcorbé, V., Benitez-Nelson, C. R., Masqué, P., Verdeny, E., White, A. E., Popp, B. N., et al. (2015). Small phytoplankton drive high summertime carbon and nutrient export in the gulf of California and Eastern tropical north pacific. *Global Biogeochem. Cycles.* 29, 1309–1332. doi: 10.1002/2015GB005134

R Core Team (2021). *R: a language and environment for statistical computing.*

Riebesell, U., Czerny, J., von Bröckel, K., Boxhammer, T., Büdenbender, J., Deckelnick, M., et al. (2013). Technical note: a mobile sea-going mesocosm system – new opportunities for ocean change research. *Biogeosciences* 10, 1835–1847. doi: 10.5194/bg-10-1835-2013

Rijkenberg, M. J. A., Middag, R., Laan, P., Gerringa, L. J. A., Van Aken, H. M., Schoemann, V., et al. (2014). The distribution of dissolved iron in the West Atlantic ocean. *PloS One*, 9, e101323. doi: 10.1371/journal.pone.0101323

Riley, J. S., Sanders, R., Marsay, C. M., Le Moigne, F. A. C., Achterberg, E. P., and Poulton, A. J. (2012). The relative contribution of fast and slow sinking particles to ocean carbon export. *Global Biogeochem. Cycles*, 26. doi: 10.1029/2011gb004085

Ristow, G. H. (1997). Wall correction factor for sinking cylinders in fluids. *Phys. Rev. E.* 55, 2808–2813. doi: 10.1103/PhysRevE.55.2808

Roberts, E. C. (2003). Response of temperate microplankton communities to N:Si ratio perturbation. *J. Plankton. Res.* 25, 1485–1495. doi: 10.1093/plankt/fbg109

RStudio Team (2022). *RStudio: integrated development environment for r.*

Sanders, R., Morris, P. J., Poulton, A. J., Stinchcombe, M. C., Charalampopoulou, A., Lucas, M., et al. (2010). Does a ballast effect occur in the surface ocean. *Geophys. Res. Lett*, 37. doi: 10.1029/2010gl042574

Sarmiento, J. L., Gruber, N., Brzezinski, M. A., and Dunne, J. P. (2004). High-latitude controls of thermocline nutrients and low latitude biological productivity. *Nature* 427, 56–60. doi: 10.1038/nature02127

Sarmiento, J. L., Simeon, J., Gnanadesikan, A., Gruber, N., Key, R. M., and Schlitzer, R. (2007). Deep ocean biogeochemistry of silicic acid and nitrate. *Global Biogeochem. Cycles.* 21. doi: 10.1029/2006GB002720

Sarthou, G., Baker, A. R., Blain, S., Achterberg, E. P., Boye, M., Bowie, A. R., et al. (2003). Atmospheric iron deposition and sea-surface dissolved iron concentrations in the eastern Atlantic ocean. *Deep. Sea. Res. Part I.: Oceanogr. Res. Papers.* 50, 1339–1352. doi: 10.1016/S0967-0637(03)00126-2

Sharp, J. H. (1974). Improved analysis for "particulate" organic carbon and nitrogen from seawater. *Limnol. Oceanogr.* 19, 984–989. doi: 10.4319/lo.1974.19.6.0984

Siegel, D. A., DeVries, T., Doney, S. C., and Bell, T. (2021). Assessing the sequestration time scales of some ocean-based carbon dioxide reduction strategies. *Environ. Res. Lett.* 16, 104003. doi: 10.1088/1748-9326/ac0be0

Smetacek, V. (1985). Role of sinking in diatom life-history cycles: ecological, evolutionary and geological significance. *Mar. Biol.* 84, 239–251. doi: 10.1007/bf00392493

Smetacek, V. (1999). Diatoms and the ocean carbon cycle. *Protist* 150, 25–32. doi: 10.1016/s1434-4610(99)70006-4

Sommer, U. (1994). Are marine diatoms favoured by high Si:N ratios? *Mar. Ecol. Prog. Ser.* 115, 309–315. doi: 10.3354/meps115309

Taucher, J., Arístegui, J., Bach, L. T., Guan, W., Montero, M. F., Nauendorf, A., et al. (2018b). Response of subtropical phytoplankton communities to ocean acidification under oligotrophic conditions and during nutrient fertilization. *Front. Mar. Sci.* 5. doi: 10.3389/fmars.2018.00330

Taucher, J., Jones, J., James, A., Brzezinski, M. A., Carlson, C. A., Riebesell, U., et al. (2015). Combined effects of CO_2 and temperature on carbon uptake and partitioning by the marine diatoms thalassiosira weissflogii and *Dactyliosolen fragilissimus*: combined effects of CO_2 and temperature. *Limnol. Oceanogr.* 60, 901–919. doi: 10.1002/lno.10063

Taucher, J., Stange, P., Algueró-Muñiz, M., Bach, L. T., Nauendorf, A., Kolzenburg, R., et al. (2018a). In situ camera observations reveal major role of zooplankton in modulating marine snow formation during an upwelling-induced plankton bloom. *Prog. Oceanogr.* 164, 75–88. doi: 10.1016/j.pocean.2018.01.004

Tonnard, M., Planquette, H., Bowie, A. R., van der Merwe, P., Gallinari, M., Desprez De Gésincourt, F., et al. (2020). Dissolved iron in the north Atlantic ocean and Labrador Sea along the GEOVIDE section (GEOTRACES section GA01). *Biogeosciences* 17, 917–943. doi: 10.5194/bg-17-917-2020

Trainer, V. L., Bates, S. S., Lundholm, N., Thessen, A. E., Cochlan, W. P., Adams, N. G., et al. (2012). Pseudo-nitzschia physiological ecology, phylogeny, toxicity, monitoring and impacts on ecosystem health. *Harmful. Algae.* 14, 271–300. doi: 10.1016/j.hal.2011.10.025

Volk, T., and Hoffert, M. I. (1985). Ocean carbon pumps: analysis of relative strengths and efficiencies in ocean-driven atmospheric CO_2 changes. *Geophys. Monogr.* 32, 99–110. doi: 10.1029/GM032p0099

Wickham, H., Averick, M., Bryan, J., Chang, W., D'Agostino McGowan, L., François, R., et al. (2019). Welcome to the tidyverse. *J. Open Source Software.* 4, 1686. doi: 10.21105/joss.01686

Xiang, Y., Lam, P. J., Burd, A. B., and Hayes, C. T. (2022). Estimating mass flux from size-fractionated filtered particles: insights into controls on sinking velocities and mass fluxes in recent U.S. GEOTRACES cruises. *Global Biogeochem. Cycles.* 36. doi: 10.1029/2021GB007292